New Journal of Physics
The open-access journal for physics

Metallic properties of magnesium point contacts

R H M Smit[1], A I Mares[1,4], M Häfner[2,3], P Pou[3], J C Cuevas[3] and J M van Ruitenbeek[1,5]

[1] Kamerlingh Onnes Laboratorium, Leiden University, PO Box 9504, NL-2300 RA Leiden, The Netherlands
[2] Institut für Theoretische Festkörperphysik and DFG—Center for Functional Nanostructures, Universität Karlsruhe, D-76128 Karlsruhe, Germany
[3] Departamento de Física Teórica de la Materia Condensada, Universidad Autónoma de Madrid, E-28049 Madrid, Spain
E-mail: ruitenbeek@physics.leidenuniv.nl

New Journal of Physics **11** (2009) 073043 (13pp)
Received 21 April 2009
Published 23 July 2009
Online at http://www.njp.org/
doi:10.1088/1367-2630/11/7/073043

Abstract. We present an experimental and theoretical study of the conductance and stability of Mg atomic-sized contacts. Using mechanically controllable break junctions (MCBJ), we observed that the room temperature conductance histograms exhibit a series of peaks, which suggests the existence of a shell effect. Its periodicity, however, cannot be simply explained in terms of either an atomic or electronic shell effect. We also found that at room temperature, contacts of the diameter of a single atom are absent. A possible interpretation could be the occurrence of a metal-to-insulator transition as the contact radius is reduced, in analogy with what is known in the context of Mg clusters. However, our first principles calculations show that while an infinite linear chain can be insulating, Mg wires with larger atomic coordinations, as in realistic atomic contacts, are always metallic. Finally, at liquid helium temperature, our measurements show that the conductance histogram is dominated by a pronounced peak at the quantum of conductance. This is in good agreement with our calculations based on a tight-binding model that indicated that the conductance of a Mg one-atom contact is dominated by a single fully open conduction channel.

[4] Current address: Nederlands Meetinstituut, PO Box 654, NL-2600 AR Delft, The Netherlands.
[5] Author to whom any correspondence should be addressed.

Contents

1. Introduction

The understanding of conductance at the very small scale of a single atom has advanced greatly over the last decade due to a joint effort from both experiment and theory [1]. In this regime, the total conductance, G, is described by the Landauer formula: $G = G_0 \sum_{i=1}^{N} \tau_i$, where $G_0 = 2e^2/h$ is the quantum of conductance and τ_i is the value of transmission for the ith electronic mode (channel). For many metals, the conductance of a one-atom contact does not match the value of a single quantum of conductance. Values in excess of $2e^2/h$, found for transition metal contacts, indicate that the conductance has to be determined by multiple channels. A pivotal contribution to the understanding of these single-atom contacts was given by Scheer *et al* [2]. They showed that the maximum number of modes to be considered was limited by the number of valence orbitals of the central atom [3].

In the case of s^1 metals, such as the alkali and noble metals, the conduction is given by a single electronic mode. Experimentally, the transmission of this 'channel' is found to be close to one, resulting in a conductance close to $2e^2/h$ or a resistance of 13 kΩ. For sp metals, the total conduction is governed by three channels, but this does not lead to a conductance of 3 G_0, since the electronic states in general have a transmission $\tau < 1$. For the transition metals, the number of conduction channels even increases to five, due to the d orbitals.

When we shift our attention to Mg, however, it is not so easy to predict what the conductance through the single atom will be. An isolated atom of this s^2 metal has the s-shell fully filled, but the p-shell is still empty. It is therefore not straightforward to predict which electronic states are of importance to the conductance of a single-atom contact. A comparable electronic structure can be found in Zn, where the 4s-shell is completely filled while the 4p-shell is empty. Häfner *et al* [4] have shown that the conductance of a single-atom contact in this case was between 0.8 and 1.0 G_0, where the transmission was largely given by a single channel.

The fact that bulk Mg is a metal results from the hybridization of the 3s and the 3p bands that originates from the large coordination number (12 in an hcp structure). However, the situation might be different when this coordination is reduced. Indeed, it is well known that Mg clusters exhibit unusual properties (see [5] and references therein). In particular, it has been shown that the nonmetallic-to-metallic transition in Mg clusters is non-monotonic and clearly slower than, for instance, that in alkali metals [6]. This is due to the dramatic change in the electronic structure of Mg with the number of interacting atoms. In the extreme case of a dimer,

the bonding is due to weak van der Waals interactions. In the thinning of an atomic contact there is a progressive reduction of the coordination of the atoms and, with it, the hybridization. In this sense, the first question we want to address in this work is whether this reduction is enough to induce a metal-to-insulator transition for small Mg contacts.

Besides the crossover from insulating to metallic behaviour, cluster experiments also demonstrated a shell structure [6]. One speaks of a shell structure if the mass spectrum shows a periodicity as a function of the radius [7]. The first observation of a shell structure in magnesium clusters was found to be due to the closing of facets and the crystalline arrangement [8]. The hexagonally close-packed lattice leads to the periodic occurrence of highly stable icosahedrons. Later experiments performed with magnesium in supercold helium droplets showed shell structure due to the delocalized electrons that display electronic level bunching [9].

Analogies to cluster shell structures were already found in quantum point contacts of alkali metals [10] and subsequent work showed that these are not limited to this chemical group [11, 12]. For metallic contacts to demonstrate shell structures, the atoms require sufficient thermal energy in order to find the local minima in energy. For sodium, the necessary temperature for observing the shell effects was found to be around 80 K [13]. Since magnesium has a much higher melting temperature (922 K versus 371 K for Na), one expects the necessary temperature in this case to be above 200 K. The second question we want to address therefore is whether magnesium point contacts demonstrate shell structures at room temperature. The fact that small clusters are insulating, while small contacts have their electronic structure influenced by the leads, makes the comparison between the two manifestations of the shell structures all the more interesting.

This paper is organized as follows. In section 2, we describe the experimental technique used in this work to study the mechanical and transport properties of Mg atomic-sized contacts. Then, in section 3, we discuss our observations at room temperature, which suggest the existence of a shell effect. Section 4 is devoted to a theoretical analysis of Mg nanocontacts. In particular, we present first principles calculations of the electronic structure of Mg infinite wires of different thicknesses as well as conductance calculations for Mg one-atom contacts based on a tight-binding model. In section 5, we discuss our experimental results for the conductance of Mg point contacts at liquid helium temperature. Finally, we summarize, in section 6, the main conclusions of our work.

2. Experimental technique

In order to investigate Mg contacts experimentally, we have used mechanically controllable break junctions (MCBJ) at both room temperature and liquid helium temperature. We start with a magnesium wire (purity better than 99.9%) of 125 μm diameter and about 15 mm length and give this wire a small incision in the middle.

For the low-temperature measurements, the wire is glued on top of an insulating Kapton layer, which covers a phosphor bronze bendable substrate. The glue (Stycast Epoxy 2850FT with curing agent 24LV) is positioned on either side and is as close to the incision as possible. The bendable substrate is clamped in a three-point bending configuration inside a vacuum pot that is brought to a pressure $<10^{-5}$ mbar. The pumping is done by an oil-free diaphragm pump in combination with a turbo molecular pump to reduce possible contamination, especially by hydrogen. This is important, considering the strong chemical affinity of magnesium for hydrogen [14]. After pumping, the vacuum pot is submerged in liquid helium, cooling the

sample down to a temperature close to 4.2 K. An important benefit of this technique is that it maintains the sample in a cryogenic vacuum and minimizes the possibility of contamination. Using a mechanical axis for the coarse movement, the wire is broken at the incision. In this way, the two electrodes are formed by freshly exposed surfaces, which is critical for the study of reactive materials such as magnesium. A stacked piezo element is used for the fine adjustments of the contact diameter during the experiment. By relaxing the bending of the substrate, the two clean surfaces can be brought into contact again, adjusting the size of the contact to the level of single atoms.

The setup we have used to study magnesium at room temperature is comparable to the one used at low temperatures [15]. Instead of one substrate, we now use two, fixed inline with a small gap as separation. In this way, both the substrates can act as separate electrodes, avoiding the need for insulation of the wire. The magnesium wire is stretched across the gap at the top and fixed by small clamps on either side. One thus avoids the use of glue, which can cause problems in the combination with ultrahigh vacuum (UHV). The piezo is positioned below the gap and presses the two substrates upward and outward, effectively breaking the wire. The ratio between the upward movement of the piezo and the outward stretching of the sample wire (commonly called the reduction ratio) is comparable to the low-temperature configuration, resulting in a similar stability. The sample holder with the wire is mounted on a stainless steel insert, which is inserted from the top into the UHV chamber. The chamber is pumped down to 10^{-7} mbar with a turbo pump; after this, it is baked at 450 K. In combination with an ion pump, the pressure can be brought down to 1×10^{-10} mbar. During the measurement, however, the turbo pump is shut down to minimize the mechanical vibrations coupling to the sample. The base pressure during the experiments is 4×10^{-10} mbar.

The level of contamination in both these setups is too low to have an influence on the results. This can be concluded from the data being reproducible during a period of several days. Since the sample configuration is comparable in both setups, their difference is limited to the temperature. The surface diffusion of atoms at low temperatures is frozen out, forcing the contact to the nearest low-energy state in configuration space. At room temperature, however, thermal diffusion of the atoms allows the contact to probe a wider range of configurations. Subtle energy differences such as the one caused by the shell effect are then probed more effectively.

3. Room temperature results

The evolution of conductance when breaking the wire at room temperature has a characteristic that can be seen in the example of figure 1(a). We see a step-like lowering of the conductance towards zero with stretching of the wire. Relatively stable intervals or plateaus occur when the mechanical tension on the contact gradually builds up. When this tension is released by a mechanical reconfiguration of the contact, its diameter and conductance are reduced stepwise [16]. The plateaus in conductance appear flat and the jumps during the mechanical reconfigurations are large. This is an indication that some values of conductance are stabilized when they are related to structures with a local minimum in the energy.

In order to verify that these plateaus occur at reproducible values, we use a statistical description by means of a conductance histogram [17]. This histogram is constructed by dividing the conductance interval of interest into equal sub-intervals or bins. For each measured

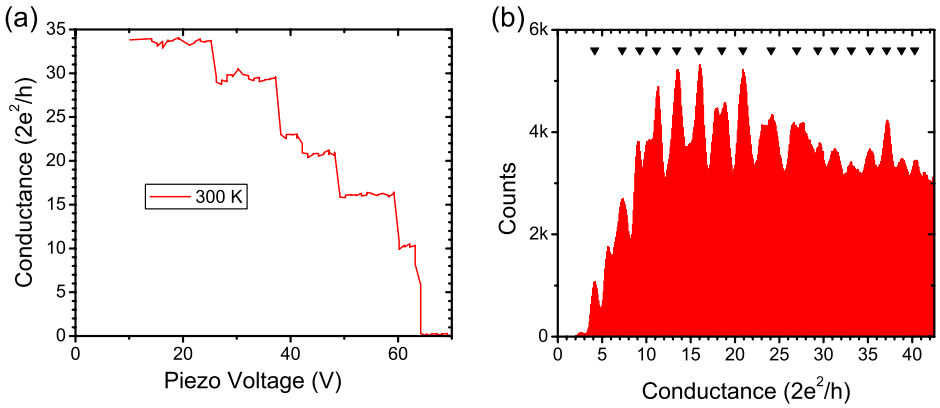

Figure 1. (a) The conductance evolution during the stretching of a magnesium contact at room temperature in UHV. The conductance was measured at a bias voltage of 20 mV. (b) A conductance histogram resulting from 1.2×10^4 of these traces. The resolution of this histogram was set to 10 bins per G_0. The conductance peaks, obtained by an automatic procedure, are indicated by arrows at the top of the panel.

data point, we determine the corresponding bin, resulting in a probability distribution for the conductance during breaking. An example of such a distribution or histogram for Mg is given in figure 1(b). We varied the speed of the electrode separation between 1.0 and 5.0×10^1 nm s^{-1}, but this had no significant effect on the conductance histograms.

The result of figure 1 indeed shows a series of peaks at higher conductance values. The positions of these peaks were determined automatically by a numerical procedure registering changes in the sign of its numerical derivative. The obtained values are indicated by arrows in the figure. These could indicate the presence of a shell structure, but in order to investigate whether the peaks in figure 1 are indeed periodic in the radius, we need to plot the histogram as a function of the radius, R. Since the range of conductances in this graph corresponds to the ballistic conductance regime, we can obtain the R from G via the corrected Sharvin formula

$$G \approx G_0 \left[\left(\frac{k_F R}{2} \right)^2 - \frac{k_F R}{2} + \frac{1}{6} + \cdots \right], \tag{1}$$

where k_F represents the Fermi wave vector [18, 19].

For the specific case of figure 1, the calculated radius for the peaks is plotted in figure 2. The obtained data points are clearly described by two linear fits, indicating a crossover between two shell effects with different periods [10]. For this specific histogram, the period changes from $1.6\,(k_F R)^{-1}$ for small contact diameters to $3.2\,(k_F R)^{-1}$ for larger contact diameters.

To compare these values to the periodicity expected for shell structures due to atomic packing, one can start from a simple packing model for a close-packed hexagonal lattice and increase the contact diameter facet by facet. One then obtains a periodicity of $2.3\,(k_F R)^{-1}$, which is only slightly influenced, considering other crystal structures such as a face (body)-centred cubic. In figure 2, this period is represented by the dotted line, which is clearly deviating from the obtained data.

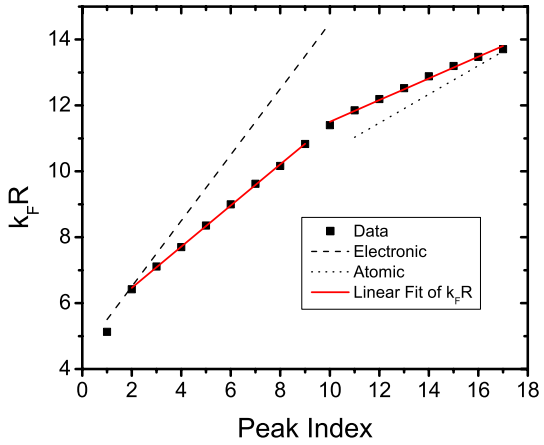

Figure 2. Graph showing the value for $k_F R$ obtained for the conductance peaks in figure 1. The data points are successfully described by two linear fits, indicating a periodicity of 1.6 $(k_F R)^{-1}$ at smaller contact diameters and 3.2 $(k_F R)^{-1}$ at bigger contact diameters. Two additional lines indicate the expected periodicity for atomic (dotted) and electronic (dashed) shell effects as described in the text.

Possible electronic shell structures have been studied for metallic point contacts as well. Both calculations using jellium models [20] and nanoscale free-electron models [21] applied to aluminium point contacts [12], give frequencies up to 1 $(k_F R)^{-1}$. As the frequencies for Mg are suggested to be the same as that for Al [21], we represent this period by a dashed line in figure 2. Since none of the lines provide a good description of the data, the shell effects seen in the experiment are still without satisfactory explanation. One possibility is that the contact is governed by competing effects of the atomic packing and the electronic free energy simultaneously. Similar mixed structures were also found for Mg clusters [22].

In our experiments on the whole, more than 90% of the measured histograms for all six samples at room temperature show a periodicity in $k_F R$, but the observed frequencies in the total conductance interval vary in the range of 1–3.5 $(k_F R)^{-1}$. In 50% of the histograms, we obtained a value around 1.7 $(k_F R)^{-1}$ for lower conductance values. At higher conductance values there is almost always a crossover to higher frequencies. The frequency at this second conductance interval varies strongly and often there are multiple frequencies superimposed. This indeed makes it likely that the shell effect is the result of multiple properties of the metal.

Another feature of the histogram in figure 1 that is even more remarkable is the absence of plateaus below 5 G_0. This minimal value is much higher than for all other metals studied with this technique [11, 12, 15]. Below this threshold value, we only found a smooth exponential decrease in conductance, typical for tunnelling behaviour. In principle, this suggests that smaller contacts are not stable. However, from the analysis of the data, we cannot exclude that a metal-to-insulator transition is taking place. As we explained in section 1, as the contact radius is reduced, the overlap between the s and p states of the atoms in the constriction decreases. Such a decrease could potentially lead to the opening of a gap in the Mg density of states (DOS). In the next section, we present a theoretical analysis to elucidate this issue.

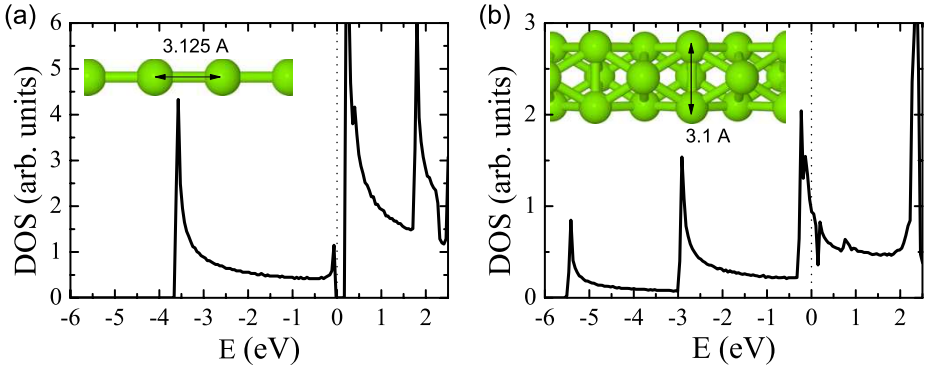

Figure 3. DOS of Mg wires calculated with CASTEP [23] for (a) a linear chain with an optimal interatomic distance of 3.125 Å and (b) an infinite wire with a three atoms cross section. The wire is built up along the *c*-axis keeping the bulk symmetry as shown in the inset. The interatomic distance that minimizes the total energy is 3.1 Å.

4. Theory

The numerous existent theoretical results on Mg clusters (see [22] and references therein) cannot be used to resolve the problem of whether or not a Mg point contact can become insulating. A metal-to-insulator transition is well defined only for truly infinite systems. Thus, in order to shed light on this problem, we have studied the stability and electronic structure of a series of Mg infinite wires with small coordination numbers. To be precise, we have carried out density functional theory (DFT) calculations of the structural and electronic properties of Mg wires ranging from the smallest possible coordination, two in the case of a chain, to 6. In the insets of figure 3, we present two examples of the configurations of the studied wires. In panel (a) one can see a linear chain, while panel (b) shows an infinite wire with a cross section of three atoms (coordination number is equal to 6) grown along the *c*-axis of an hcp bulk structure and keeping the bulk relative positions.

For these *ab initio* calculations, we have used a standard implementation of DFT [24, 25] with a plane wave basis set and ultrasoft pseudopotentials [26]. The Perdew–Burke–Ernzerhof approach (PBE) [27] has been chosen for the exchange–correlation contribution. The calculations were performed with the CASTEP v4.2 code [23]. The plane wave cutoff used (375 eV) in all our calculations assures us of well-converged structural and electronic properties. The convergence criteria for the atomic relaxations involved in the different calculations are 0.01 eV $Å^{-1}$ for the mean value of the forces, 0.001 Å for the atomic positions and 10^{-6} eV for the total energy. We have used a cubic supercell of four atoms for the linear chain and two atomic layers for the wire adding a vacuum of 10 Å in the directions perpendicular to the wires. We have optimized, by minimizing the system energy, the interatomic distances of the wires keeping the original symmetry with a Monkhorst–Pack (MP) $\vec{k}$-sampling mesh of $1 \times 1 \times 64$ [28]. The DOS has been calculated with a mesh of $1 \times 1 \times 1024$.

Turning to the results, in the two systems shown in figure 3, we have found interatomic distances (3.1 Å) slightly smaller than the bulk value (3.2 Å) in accordance with calculations of Mg clusters [22]. In figure 3(a), we show the DOS of the linear chain for the optimized

interatomic distance[6]. A small gap of 0.3 eV is observed; consequently, the linear chain does not show metallic behaviour. However, even for this wire with the lowest coordination number, the broadening due to the 3s–3p hybridization has nearly closed the gap. Indeed, we have found that all the wires with larger coordination than the linear chain are metallic. The DOS of a wire with a cross section of three atoms is shown in figure 3(b); it does not exhibit any gap. In fact, up to five different bands cross the Fermi level. We have investigated whether the application of some additional stress will modify these results, but we have found that even with an increase of the interatomic distances by 10%, the wires remain metallic. So, in short, from this analysis we do not expect the formation of insulating Mg wires in the last stages of the breaking of Mg contacts.

The results above show that low-coordinated Mg structures are, in principle, stable, which suggests that the formation of few-atom contacts might be possible, at least at low temperatures. Moreover, since these structures are metallic, the following question naturally arises: what is the expectation for the linear conductance of the smallest Mg contacts? In order to answer this question, we have computed the conductance of Mg one-atom contacts within the Landauer formalism. For this purpose, we have combined the tight-binding parameterization of [29] with non-equilibrium Green's function techniques. This approach has been very successful in describing the transport properties of a great variety of metallic atomic-sized contacts [30]–[33]. We proceed to briefly explain it. In this approach, the electronic structure of the atomic contacts is described in terms of the following Hamiltonian written in a nonorthogonal local basis:

$$\hat{H} = \sum_{i\alpha,j\beta,\sigma} H_{i\alpha,j\beta}\hat{c}^{\dagger}_{i\alpha,\sigma}\hat{c}_{j\beta,\sigma}, \tag{2}$$

where i and j run over the atomic sites, α and β denote different atomic orbitals, σ is the spin and $H_{i\alpha,j\beta}$ are the on-site energies ($i = j$) or hopping elements ($i \neq j$). Additionally, we need the overlap integrals $S_{i\alpha,j\beta}$ of orbitals at different atomic positions. We take these matrix elements from the tight-binding parameterization of [29], which is designed to accurately reproduce the band structure of bulk materials. The atomic basis is formed by nine valence orbitals, namely the s, p and d orbitals which give rise to the main bands around the Fermi energy. In this parameterization, both the hoppings and the overlaps are functions of the atomic distances, which have a cutoff radius that encloses up to 13 nearest-neighbour shells. Finally, in order to take into account the low coordination in the smallest atomic contacts, we impose local charge neutrality through the self-consistent variation of the on-site energies of the atoms in the constrictions.

With the help of Green's function techniques, one can translate the information on the electronic structure contained in the Hamiltonian of equation (2) into the conductance of these atomic junctions (see [31, 33] for details). As explained in section 1, this low-temperature conductance adopts the form of the Landauer formula

$$G = G_0 T(E_F) = G_0 \sum_n \tau_n, \tag{3}$$

[6] We have studied the stability of the linear chain allowing the four atoms of the supercell to relax starting from a zigzag configuration. For cell lengths larger than 10.5 Å, the final configuration is a linear chain that is slightly distorted, with an energy minimum corresponding to an interatomic distance of 3.125 Å and a zigzag angle of 177°. The stable solution for smaller supercell lengths is a compressed zigzag chain where the atoms have four nearest neighbours with an interatomic distance of 3.1 Å.

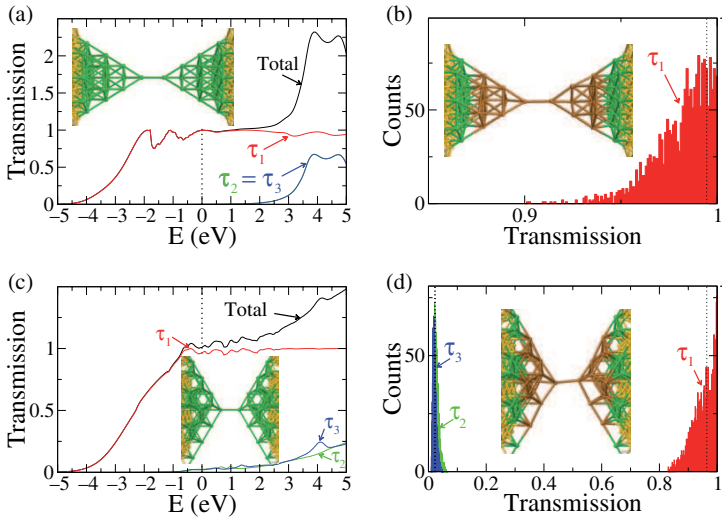

Figure 4. (a) Total transmission and transmission coefficients as a function of energy for the contact shown in the inset. This geometry is grown along the [0001] direction (c-axis); it contains a dimer in its central part and the interatomic distances are fixed at the bulk values. The yellow atoms correspond to atoms in the semi-infinite surfaces that are used to model the leads. The transmission coefficients at the Fermi energy (set as zero and indicated with a dotted vertical line) are $\tau_1 = 0.993$, $\tau_2 = \tau_3 = 0.76 \times 10^{-3}$ and the total conductance is $\sim 0.995\, G_0$. (b) Histograms of the transmission coefficients for 2000 disorder realizations (see text) of the one-atom contact of the inset of panel (a). The brown atoms are those that have been randomly displaced. The vertical dotted lines indicate the values of the transmission coefficients for the ideal geometry. The transmission values of the second and third channels remain below 2×10^{-3} and are not shown. (c) Same as panel (a), but for the contact grown along the [11 $\bar{2}$0] direction (a-axis) shown in the inset. The total conductance is $\sim 1.01\, G_0$ with $\tau_1 = 0.9640$, $\tau_2 = 0.024$, $\tau_3 = 0.021$ and $\tau_4 = 0.3 \times 10^{-3}$. (d) Same as panel (b) for the contact in the inset of panel (c).

where $G_0 = 2e^2/h$ denotes the quantum of conductance, E_F the Fermi energy and τ_n the transmission of the nth transmission eigenchannel at E_F.

We now turn to analysis of the results for the linear conductance of some ideal, and yet plausible, one-atom geometries, which have been chosen to simulate what may happen at the last conductance plateau before the rupture of the nanowires. In the inset of figure 4(a), we show an example of a one-atom contact grown along the [0001] direction (c-axis), which contains a dimer in its central part. Different molecular dynamics simulations of atomic contacts of various metals have suggested that this type of geometry is realized very frequently at the last plateau [31, 33, 34]. This particular geometry is constructed starting with the dimer and choosing the nearest neighbours in the next layers. Finally, the leads are modelled as infinite surfaces grown along the same direction (yellow atoms in the inset of figure 4(a)). In this ideal case, all interatomic distances are fixed to their bulk values, which is justified by the *ab initio* calculation of Mg clusters [22] and our results for infinite wires presented above. The

total transmission and the individual transmission coefficients, τ_i, for this contact are shown in figure 4(a) as a function of energy. The first thing to notice is the fact that the system is metallic, in accordance with our expectations based on the DFT results described above. Furthermore, as one can see, the conductance, which is determined by the transmission at E_F, is very close to $1\,G_0$ and is completely dominated by a single fully open channel. The second and third channels, which are degenerate due to the symmetry of the contact, have transmissions below 10^{-3}. One can get a deeper insight into these results and, in particular, into the nature of the conduction channels, by analysing the local DOS projected onto the different orbitals of the two central atoms (not shown here). Such an analysis indicates that the dominant channel is formed by a symmetric (bonding) combination of the s and p_z orbitals of the central atoms (z is the transport direction), while the p_x and p_y orbitals are responsible for the second and third channels. A fourth channel, which in this case has a transmission below 10^{-5}, is formed by the antisymmetric combination of the s and p_z orbitals. Such an anti-bonding combination is basically orthogonal to incoming states (from the leads) and therefore does not contribute significantly to the transport. So, in short, these results resemble very much what happens in the case of Zn one-atom contacts [4] and also in the case of the final stages of the last plateau of Al contacts [35, 36]. This is, after all, quite reasonable since, in all these cases, the electronic structure at the Fermi energy is governed by the s and p orbitals.

Since we do not exactly know the growth direction of the Mg atomic contacts, we have studied the conductance of geometries with different crystallographic orientations. In figure 4(c), we present another example of a dimer contact, but this time grown along the $[11\bar{2}0]$ direction (a-axis). Note that the total conductance and the transmission coefficients are similar to those of the [0001] case, the main difference being the larger values for the second and third channels and the lifting of their degeneracy. While the lack of degeneracy reflects the lower symmetry of the contacts in the $[11\bar{2}0]$ direction, the larger transmission values can be attributed to the larger apex angle of those contact geometries and, in consequence, a stronger coupling of the dimer atoms and next layers.

In principle, the contact geometries should be determined from molecular dynamic simulations, but this is computationally very demanding. Instead, and in order to test the robustness of our results, we have studied the role of disorder in the atomic positions. For this purpose, starting from the ideal geometries of figures 4(a) and (c), we have changed randomly the positions of the atoms in the constriction region (those highlighted in brown in figures 4(b) and (d)) with a maximum amplitude of $\pm 5\%$ of the nearest-neighbour distance. Then, we have computed the total transmission and the transmission coefficients of the disorder geometries, and the results are shown in the form of histograms in figures 4(b) and (d). As one can see, in both cases the conductance is still dominated by a single channel that is almost fully open. Therefore, these results confirm our basic conclusion, namely the fact that a Mg one-atom contact is expected to have a conductance close to $1\,G_0$ dominated by a single channel.

5. Low-temperature results

In order to test this latter conclusion of our theoretical analysis, we repeated the experiments at low temperatures. Here, we broke the contact by ramping the piezo element continuously with a speed of $1.8 \times 10^3\,\mathrm{V\,s^{-1}}$ (corresponding to $1.0 \times 10^2\,\mathrm{nm\,s^{-1}}$ electrode separation). This resulted in traces as the one shown in figure 5(a). The plateaus in conductance appear more structured and the jumps during the mechanical reconfigurations are smaller than those measured at

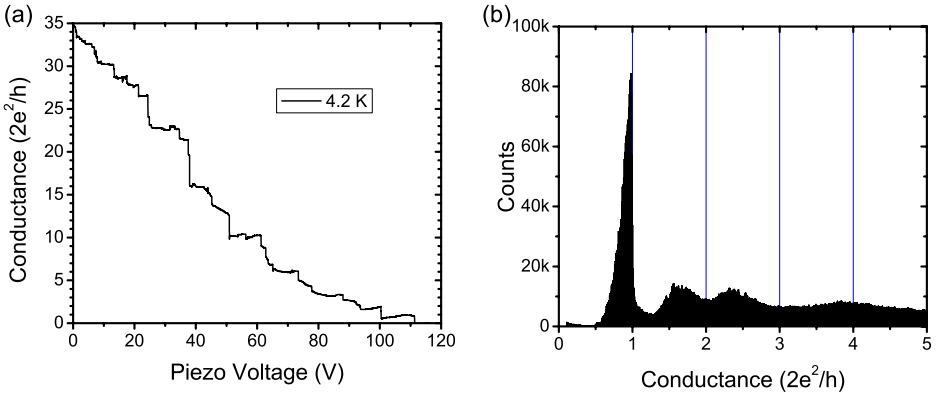

Figure 5. Figure comparable to figure 1, but for a measurement performed at liquid helium temperature. Panel (a) shows the conductance evolution measured at a bias voltage of 100 mV. Panel (b) shows a conductance histogram resulting from 3×10^3 of these traces. The resolution of this histogram was set to 115 bins per G_0.

room temperature. In the conductance histogram, presented in figure 5(b), this results in a flat distribution at higher conductance values. The shell structures found at room temperature are thus absent at low temperatures, as we had expected.

When focusing on the trace at low conductance values, the staircase of plateaus indeed continues down to values below 5 G_0. The histogram, the shape of which was reproduced over a set of ten different samples, shows its lowest conductance peak close to 1 G_0. For a minority of the histograms, a shoulder down to values as low as 0.8 G_0 is seen. In rare cases, this shoulder even grows to form the primary peak. Although the conductance does not reveal information on the individual values of transmission, τ_i, of the electron states, the strong asymmetry and the closeness of the peak to 1 G_0 do suggest that its conductance is given by only one, almost fully opened, channel. For multiple channels, the value of 1 G_0 would not form a fundamental limit.

This result agrees nicely with our calculations for the conductance of Mg single-atom contacts. The properties of Mg at low temperatures are therefore very close to the results obtained previously for Zn [4]. The most noticeable differences are the absence of data points between 0.5 G_0 and tunnelling and the higher relative intensity of the peak close to 1 G_0 in the case of Mg. The presence of this peak indicates that the instability of small point contacts at room temperature is not related to a metal-to-insulator transition.

6. Conclusions

In conclusion, magnesium contacts at room temperature demonstrate shell effects at multiple frequencies. The most frequent and intense frequency of 1.7 $(k_F R)^{-1}$ did not match with either the expected frequency for atomic packing or the previously calculated frequencies for electronic shell structures. This value therefore remains without satisfactory explanation. One possibility is that both effects play an important role at the same time.

The histograms at low temperatures exhibit a first peak close to 1 G_0. The strongly asymmetric shape of the peak, with a small weight above 1 G_0, suggests that this conductance is dominated by a single channel. Our calculations confirm this and identify this channel to be

a symmetric combination of the s and p_z orbitals of the central Mg atom. This behaviour is similar to the results obtained for Zn [4], although the tendency for the channel to be fully open is stronger.

At room temperature, contacts having the diameter of a single atom are absent. The instability of these smaller contacts is not caused by a metal-to-insulator transition at lower coordination. From the appearance of the peak at 1 G_0 at low temperatures, we can conclude that the metal–insulator transition is absent even in the smallest of contacts. Future experiments at intermediate temperatures may prove valuable for understanding these different behaviours. Our first principles calculations suggest that an infinite linear chain of Mg could be an insulator, but they also show that as soon as the coordination is larger than 2, as in any realistic contact at low temperatures, the system is metallic.

Acknowledgments

We would like to thank Gijs van Dorp and Xin-Zhou Liu for their assistance with the measurements. This work is part of the research programme 'Stichting voor Fundamenteel Onderzoek der Materie (FOM)' (RHMS, AIM and JMvR), which is financially supported by the 'Nederlandse Organisatie voor Wetenschappelijk Onderzoek (NWO)'. MH acknowledges the financial support from the KHYS and the DFG within the CFN. PP and JCC are supported by the Spanish MICINN through grant numbers MAT2008-02929/NAN and FIS2009-04209, respectively.

References

[1] Agraït N, Yeyati A L and van Ruitenbeek J M 2003 Quantum properties of atomic-sized conductors *Phys. Rep.* **377** 81–279

[2] Scheer E, Agraït N, Cuevas J C, Yeyati A L, Ludoph B, Martín-Rodero A, Bollinger G R and van Ruitenbeek J M 1998 The signature of chemical valence in the electrical conduction through a single-atom contact *Nature* **394** 154–7

[3] Cuevas J C, Yeyati A L and Martín-Rodero A 1998 Microscopic origin of conducting channels in metallic atomic-size contacts *Phys. Rev. Lett.* **80** 1066–9

[4] Häfner M, Konrad P, Pauly F, Cuevas J C and Scheer E 2004 Conduction channels of one-atom zinc contacts *Phys. Rev.* B **70** 241404

[5] von Issendorff B and Cheshnovsky O 2005 Metal to insulator transitions in clusters *Annu. Rev. Phys. Chem.* **56** 549–80

[6] Thomas O C, Zheng W, Xu S and Bowen K H 2002 Onset of metallic behavior in magnesium clusters *Phys. Rev. Lett.* **89** 213403

[7] Martin T P 1996 Shells of atoms *Phys. Rep.* **273** 199–241

[8] Martin T P, Bergmann T, Göhlich H and Lange T 1991 Evidence for icosahedral shell structure in large magnesium clusters *Chem. Phys. Lett.* **176** 343–7

[9] Diederich T, Döppner T, Braune J, Tiggesbäumker J and Meiwes-Broer K H 2001 Electron delocalization in magnesium clusters grown in supercold helium droplets *Phys. Rev. Lett.* **86** 4807–10

[10] Yanson A I, Yanson I K and van Ruitenbeek J M 2001 Crossover from electronic to atomic shell structure in alkali metal nanowires *Phys. Rev. Lett.* **87** 216805

[11] Mares A I and van Ruitenbeek J M 2005 Observation of shell effects in nanowires for the noble metals Cu, Ag and Au *Phys. Rev.* B **72** 205402

[12] Mares A I, Urban D F, Bürki J, Grabert H, Stafford C A and van Ruitenbeek J M 2007 Electronic and atomic shell structure in aluminium nanowires *Nanotechnology* **18** 265403

[13] Yanson A I, Yanson I K and van Ruitenbeek J M 1999 Observation of shell structure in sodium nanowires *Nature* **400** 144–6
[14] Sakintuna B, Lamari-Darkrim F and Hirscher M 2007 Metal hydride materials for solid hydrogen storage: a review *Int. J. Hydrog. Energy* **32** 1121–40
[15] Mares A I, Otte A F, Soukiassian L G, Smit R H M and van Ruitenbeek J M 2004 Observation of electronic and atomic shell effects in gold nanowires *Phys. Rev.* B **70** 073401
[16] Rubio G, Agraït N and Vieira S 1996 Atomic-sized metallic contacts: mechanical properties and electronic transport *Phys. Rev. Lett.* **76** 2302–5
[17] Krans J M, van Ruitenbeek J M, Fisun V V, Yanson I K and de Jongh L J 1995 The signature of conductance quantization in metallic point contacts *Nature* **375** 767–9
[18] Torres J A, Pascual J I and Sáenz J J 1994 Theory of conduction through narrow constrictions in a 3-dimensional electron-gas *Phys. Rev.* B **49** 16581–4
[19] Höppler C and Zwerger W 1998 Comment on 'Jellium model of metallic nanocohesion' *Phys. Rev. Lett.* **80** 1792
[20] Ogando E, Zabala N and Puska M J 2002 Analysis of the shell- and supershell structures of metallic nanowires with jellium models *Nanotechnology* **13** 363–8
[21] Urban D F, Bürki J, Stafford C A and Grabert H 2006 Stability and symmetry breaking in metal nanowires: the nanoscale free-electron model *Phys. Rev.* B **74** 245414
[22] Lyalin A, Solov'yov I A, Solov'yov A V and Greiner W 2003 Evolution of the electronic and ionic structure of Mg clusters with increase in cluster size *Phys. Rev.* A **67** 063203
[23] Payne M C, Teter M P, Allan D C, Arias T A and Joannopoulos J D 1992 Iterative minimization techniques for *ab initio* total-energy calculations: molecular dynamics and conjugate gradients *Rev. Mod. Phys.* **64** 1045–97
[24] Hohenberg P and Kohn W 1964 Inhomogeneous electron gas *Phys. Rev.* **136** B864–71
[25] Kohn W and Sham L J 1965 Self-consistent equations including exchange and correlation effects *Phys. Rev.* **140** A1133–8
[26] Vanderbilt D 1990 Soft self-consistent pseudopotentials in a generalized eigenvalue formalism *Phys. Rev.* B **41** 7892–5
[27] Perdew J P, Burke K and Ernzerhof M 1996 Generalized gradient approximation made simple *Phys. Rev. Lett.* **77** 3865–8
[28] Monkhorst H J and Pack J D 1976 Special points for Brillouin-zone integrations *Phys. Rev.* B **13** 5188–92
[29] Gotsis D A, Papaconstantopoulos D A and Mehl M J 2002 *Phys. Rev.* B **65** 134101
Mehl M J and Papaconsantopoulos D A 1998 Tight-binding parametrization of first-principles results *Topics in Computational Materials Science* ed C Fong (Singapore: World Scientific)
[30] Brandbyge M, Kobayashi N and Tsukada M 1999 Conduction channels at finite bias in single-atom gold contacts *Phys. Rev.* B **60** 17064–70
[31] Dreher M, Pauly F, Heurich J, Cuevas J C, Scheer E and Nielaba P 2005 Structure and conductance histogram of atomic-sized Au contacts *Phys. Rev.* B **72** 075435
[32] Viljas J K, Cuevas J C, Pauly F and Häfner M 2005 Electron–vibration interaction in transport through atomic gold wires *Phys. Rev.* B **72** 245415
[33] Pauly F, Dreher M, Viljas J K, Häfner M, Cuevas J C and Nielaba P 2006 Theoretical analysis of the conductance histograms and structural properties of Ag, Pt and Ni nanocontacts *Phys. Rev.* B **74** 235106
[34] Jelínek P, Pérez R, Ortega J and Flores F 2003 First-principles simulations of the stretching and final breaking of Al nanowires: mechanical properties and electrical conductance *Phys. Rev.* B **68** 085403
[35] Scheer E, Joyez P, Esteve D, Urbina C and Devoret M H 1997 Conduction channel transmissions of atomic-size aluminum contacts *Phys. Rev. Lett.* **78** 3535–8
[36] Cuevas J C, Yeyati A L, Martín-Rodero A, Bollinger G R, Untiedt C and Agraït N 1998 Evolution of conducting channels in metallic atomic contacts under elastic deformation *Phys. Rev. Lett.* **81** 2990–3